ISSN: 0000-0000 www.aristonpubs.com/sciengg-advances https://doi.org/10.69626/sea.2024.0056

RESEARCH ARTICLE

In_2O_3 Doped ZnO Nanosheets for Ultra-Trace Detection of NO_2

Adil Shafi Ganie †, Shahid Hussain *, Sufaid Shah †, Muhammad Javed Liaqat, Amensisa Negasa Begi, Zhenyu Miao, Yuanyuan Han

ABSTRACT: Development of facile sensors for the detection of toxic gases from the environment describes a sustainable approach for monitoring the health of ecosystem. In the current study, In_2O_3 doped ZnO based gas sensor was designed to detect the trace quantities of NO_2 gas in the environment. The synthesis of In_2O_3@ZnO nanosheets were performed by hydrothermal method. The growth of nanostructure was examined by physical and optical characterizations like X-ray diffraction and Ultra-violet diffuse reflectance spectroscopy. Microscopic studies were performed to investigate the morphological and surface structure of the nanosheets. The gas sensing experiments were carried at different temperature to examine the optimum temperature of working and it was observed the sensor worked best at 300^{O}C. The response of In_2O_3@ZnO nanosheets was seen to be significantly higher (R_g/R_a = 41.9) than pure ZnO (R_g/R_a = 14.04) at 100 ppm concentration of NO_2 gas. The higher response of In_2O_3@ZnO indicates that In_2O_3 NPs have significantly improved the potentiality of detection and response to detect NO_2. On changing concentration of NO_2 gas, the sensor showed increased response with increase in the concentration of NO_2 gas. Moreover, the sensor showed excellent selectivity, long term stability and good repeatability with lower detection limit.

Keywords: Indium oxide, Zinc oxide, In_2O_3@ZnO, NO_2 gas sensor, Nanosheet

Received: 18 February 2024; Revised: 02 April 2024; Accepted: 06 May 2024; Available Online: 23 May 2024

1. INTRODUCTION

Rise in pollution level has posed a threat to the sustainable growth of the natural environment and uncontrolled release of harmful gases into the environment has resulted in the emergence of various other environmental issues [1]. Among various gases released to the environment, Nitrogen dioxide (NO_2) is considered as hazardous gas and has potentially deleterious effects on humans and ecosystem. Long-term exposure to NO_2 at certain concentrations might raise the risk of lung illnesses and respiratory infections. Nitrogen dioxide (NO_2) is a significant air pollutant emitted from combustion processes, traffic, and industrial activities [2, 3]. Monitoring NO_2 levels is essential due to its harmful effects on human health and the environment. In this context, nanomaterial-based gas sensors have garnered significant interest due to their excellent redox and surface properties. Several semiconducting oxide materials have been extensively researched for gas sensing applications including ZnO, TiO_2, SnO_2, In_2O_3, CuO, etc and have shown high sensitivity, low detection limits, and fast response times [4, 5].

Zinc oxide (ZnO) nanosheets are a class of nanomaterials that have shown remarkable potential for plethora of applications, particularly for hazardous gas detection. Zinc oxide has a band gap of 3.37 eV and a high exciting binding energy of 60 meV at ambient temperature. ZnO has shown exceptionally good performance in electronics, optics, and photonics and has sparked a lot of research attention. ZnO is a very promising photocatalyst because of its activity, affordability, and light absorption

School of Materials Science and Engineering, Jiangsu University, China.

† Both Authors contributed equally to this work.

* Author to whom correspondence should be addressed: shahid@ujs.edu.cn (Shahid Hussain)

properties. Additionally, it has been discovered that ZnO is more effective in gas sensing due its good thermal stability, chemical stability and wide separation of conduction and valence bands [6].

ZnO is a wide-bandgap semiconductor with excellent electrical and optical properties, making it ideal for sensor development. The unique structure of ZnO nanosheets provides a high surface-to-volume ratio, enhancing the interaction between the gas molecules and the sensing material. This results in increased adsorption of target gas molecule on the exposed surface and improved sensitivity and response characteristics [7, 8]. The gas sensing mechanism of ZnO nanorods towards NO_2 is attributed to several factors. When NO_2 molecules are adsorbed onto the surface of ZnO nanorods, they undergo chemical reactions leading to changes in the electrical conductivity of the material. This change can be measured as a voltage or resistance response, allowing for the quantification of NO_2 concentration in the surrounding environment. Additionally, the high surface area of ZnO nanorods facilitates the adsorption and desorption of NO_2 molecules, contributing to the sensor's fast response and recovery times [9]. However, the gas sensing properties of ZnO faced the major drawback of lower response and lower detection limit. To overcome the obstacle, several modifications can be performed like composite formation, band gap engineering by heterostructure formation, etc.

The selectivity of ZnO nanosheets can also be tailored through surface modifications or doping with specific elements like In_2O_3, making them capable of distinguishing NO_2 from other gases commonly found in the atmosphere. Doping with In_2O_3 considerably enhance the sensor characteristics and performance with the modifications at interface chemistry [10, 11]. In_2O_3 is n-type semiconducting material with a band gap of 3.65 eV. The characteristics of In_2O_3 have been extensively investigated for gas sensing applications and can shift the performance of proposed sensor to increased levels with low interference and good selectivity [12, 13].

Moreover, significant progress has been made in optimizing the synthesis methods and structural characteristics of materials to enhance their gas sensing performance. Nowadays, sophisticated synthetic techniques such as hydrothermal growth, vapor-phase deposition, and template-assisted methods have been employed to control the size, morphology, and crystallinity of the materials, thereby improving their sensing properties [14, 15]. The comprehensive study on gas sensors based on ZnO nanostructures is said to have resulted from the simple synthesis of high-quality, single-crystalline nanostructures. The potential synthetic procedure can result in controlled morphological nanostructure with vast surface area, high chemical reactivity and high porous structure. The unique physical features of nanostructures obtained through controlled synthetic protocols have shown excellent gas sensing properties towards ethanol and NO at room temperature [16, 17]. In addition, ZnO oxides-based gas sensors may be compatible with silicon integrated circuit (IC) technology, and the metal-assisted electrode less etching approach makes the material quite reactive for gas sensing [18].

In this study, an In_2O_3 doped ZnO nanosheets were prepared by facile hydrothermal method and were pasted on electrode substrate for trace detection of NO_2 gas. The sheet like surface of In_2O_3 doped ZnO couple with efficient interface charge transfer have a profound effect on the gas sensing properties. Moreover, the structure of the nanostructures, the experimental optimizations, potential sensing mechanism and the factors influencing performance were all discussed.

2. EXPERIMENTAL DETAILS

2.1. Material and solvents: Zinc acetate dihydrate ($Zn(CH_3COOH)_2 \cdot 2H_2O$), Indium Nitrate ($In(NO_3)_3$), Sodium hydroxide (NaOH), Deionized water, Ethanol, Polyvinylpyrrolidone (PVP), Teflon-lined stainless-steel autoclave, Magnetic stirrer, Ultrasonic bath, Centrifuge, Oven.

2.2. Synthesis of ZnO and In_2O_3 doped ZnO nanosheets

The synthesis process begins with the dissolution of a specific amount of zinc acetate dihydrate in deionized water. A small amount of polyvinylpyrrolidone (PVP) is then added to the solution as a capping agent, which helps control the growth of the nanosheets and prevents agglomeration. The solution is stirred until all components are completely dissolved. Next, a 1 M solution of sodium hydroxide (NaOH) is prepared in deionized water and stirred until fully dissolved. The NaOH solution is then slowly added dropwise to the zinc precursor solution while stirring, resulting in the formation of $Zn(OH)_2$. The mixed solution is transferred to a Teflon-lined stainless-steel autoclave, which is then securely sealed. The autoclave is placed in an oven and heated to a specific temperature, usually around 80-100°C, for a period of 10-12 hours. This hydrothermal reaction leads to the formation of $Zn(OH)_2$ nanosheets. After the reaction is complete, the autoclave is allowed to cool to room temperature. The autoclave is then opened, and the formed $Zn(OH)_2$ nanosheets are carefully collected by centrifugation. The nanosheets are washed several times with ethanol and deionized water to remove any unreacted chemicals and impurities. Finally, the washed nanosheets are dried in an oven at a low temperature, around 60-80°C, to remove any remaining solvent. To convert $Zn(OH)_2$ into zinc oxide (ZnO), the sample is calcined at 600°C for 6 hours.

For the preparation of In_2O_3-doped ZnO, the process is similar to that of ZnO nanosheets. Along with zinc acetate dihydrate, a small amount of indium nitrate, approximately one-tenth of the zinc precursor, is added to the solution. The reaction is performed following the same procedure as described above.

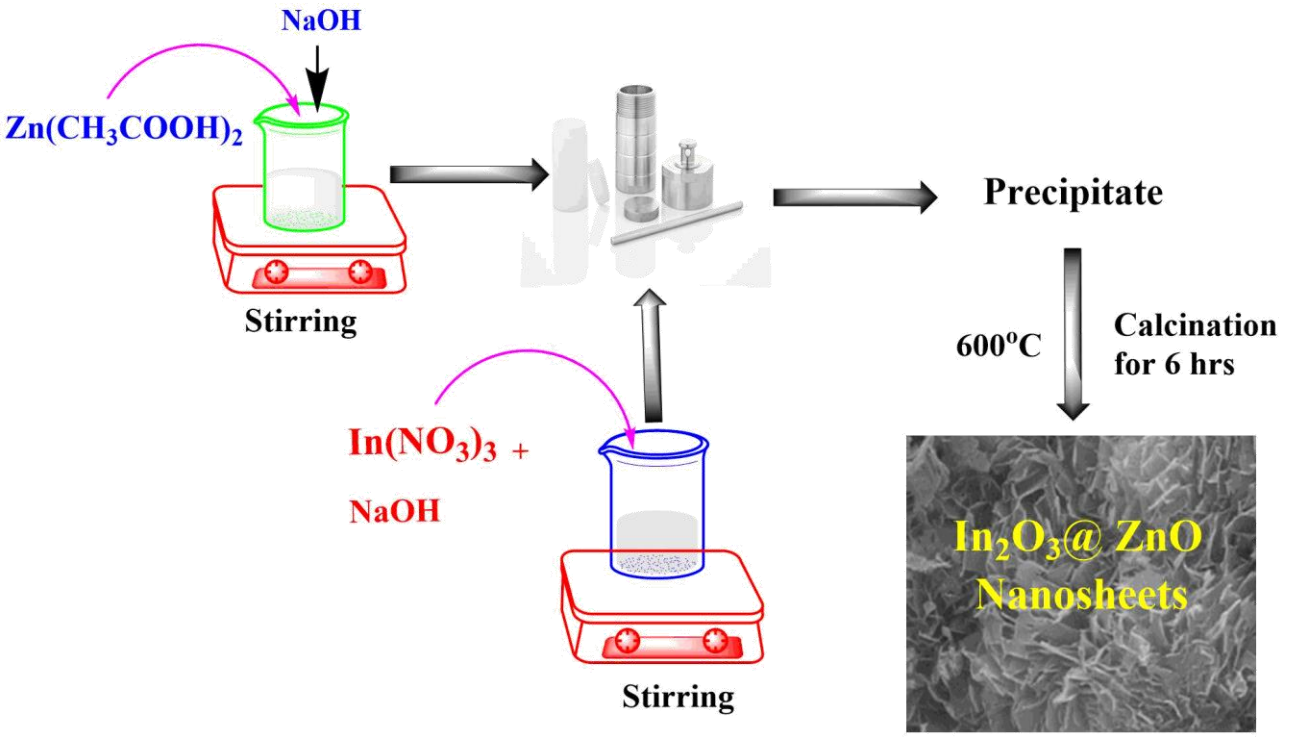

Fig. 1. Synthetic scheme of ZnO and In_2O_3@ZnO.

After calcination at 600°C for 6 hours, In_2O_3-doped ZnO nanosheets (In_2O_3@ZnO) are obtained. Figure 1 demonstrates the schematic for the synthesis of ZnO and In_2O_3@ZnO nanosheets.

2.3. Characterizations

X-ray powder diffraction was used to investigate the nanomaterial's crystalline structure by Rigaku, XRD, TTRIII, Japan. Scanning Electron Microscopy (SEM, JSM-7500, Japan) was used to get the morphological pictures of the precursors using an accelerating voltage of 10kV and an electric current of 1.0 ×10 −10 A. Topography and surface composition was determined by transmission electron microscope (TEM, H600, Japan). A specially designed chamber is used for gas sensing measurements. The gas chamber of the gas sensor testing apparatus is computer controlled to measure both the concentration and temperature of the gas. A computerized data collection system, Figaro gas sensor test chamber is an upgraded computerized was used to gather the signals from the tested and control sensors. The term "gas response" refers to the relationship between the sensor resistance in an air flow (R_a) and its steady-state resistance in an analyte gas flow (R_g). The reaction is assessed by alternating between the dry air and gas combination at 20-500 ℃.

3. RESULTS AND DISCUSSION

3.1. X-ray Diffraction analysis

X-ray diffraction studies were performed to study the crystal structure, phase composition, and crystallinity of the materials. The typical XRD spectra of ZnO and In_2O_3@ZnO are depicted in Figure 2. The spectral peaks at 2θ values of 31, 34, 36, 47, 56, 66, 69 corresponding to *hkl* value of (100), (002), (011), (012), (110), (013), (112), are well in accordance with hexagonal wurtzite structure of ZnO (Card No: 98-005-7450) [19]. The peaks in In_2O_3@ZnO are in good agreement with the ZnO with some new peaks from the In_2O_3 doping. The additional peaks at 2θ values of 66, 56, 47 and 34 corresponding to *hkl* values of (226), (044), (222), (002) in the spectra of In_2O_3 doped ZnO are be due to Indium oxide nanoparticles [19]. It can be clearly seen from the spectra of In_2O_3@ZnO, that peaks are decreased in intensity and In_2O_3 doping have caused slight shifts in the ZnO peaks due to the difference in ionic radii between Zn^{2+} and In^{3+} ions. Moreover, the crystallite size of the ZnO and In_2O_3@ZnO nanostructures has been calculated using the Scherrer equation mentioned below:

$$D = \frac{K\lambda}{\beta Cos\theta}$$

In the above equation, D is the crystallite size, K is the shape factor (typically 0.9), λ is the X-ray wavelength, β is the FWHM, and θ is the Bragg angle. The average crystallite size

obtained from the above equation was found to be in between 300 to 400 nm. However. On Indium doping the crystallite size of In_2O_3@ZnO decreased which may result in increase in the band gap.

3.2. Optical Studies

The optical properties of ZnO and In_2O_3@ZnO were thoroughly investigated using ultraviolet diffuse reflectance spectroscopy (UV-DRS), and the corresponding band gaps were determined by deriving Tauc's plots. Figure 3(a) presents the UV-DRS absorption spectra for both ZnO and In_2O_3@ZnO. It is evident from the figure that the absorption edge of pure ZnO lies within the range of 400-450 cm^{-1}, which is characteristic of the ultraviolet region. This indicates the ability of ZnO to absorb UV light effectively.

Upon doping ZnO with indium, the absorption edge of In_2O_3@ZnO shifts towards a longer wavelength, exhibiting a hypsochromic shift (blue shift). This shift suggests a modification in the electronic structure of ZnO due to the incorporation of indium ions, which can alter the band structure and consequently the optical properties of the material. The hypsochromic shift is indicative of a narrowing of the band gap, which has significant implications for the material's photocatalytic and optoelectronic applications.

To quantify the optical band gaps of ZnO and In_2O_3@ZnO, Tauc's plots were derived as shown in Figure 3(b). The band gap energies were calculated using the following equation:

$$h\nu \; F(R) = (Ah\nu - E_g)^{n/2}$$

where F(R) is the Kubelka–Munk function, h is Planck's constant, ν is the frequency, Eg is the band gap energy, and A is a proportionality constant. The value of n depends on the type of electronic transition, with n=1 for direct transitions and n=2 for indirect transitions.

From the Tauc's plots, the optical band gaps for ZnO and In_2O_3@ZnO were found to be 2.3 eV and 2.78 eV, respectively. This significant increase in the band gap for In_2O_3@ZnO compared to pure ZnO further confirms the effect of indium doping. The increase in band gap upon doping can be attributed to the alteration in the density of states near the conduction and valence bands, which affects the electronic transitions. This change in band gap is crucial as it can enhance the photocatalytic efficiency and adjust the absorption properties of the material for specific applications in UV-visible light regions.

3.3. Morphological Studies

The morphological and microstructural characteristics of the prepared samples were meticulously examined using scanning electron microscopy (SEM). The typical SEM micrographs of ZnO and In_2O_3@ZnO nanosheets are depicted in Figure 4. From these images, it is evident that the morphology of pure ZnO consists of sheet-like structures with irregular edges. These nanosheets are assembled together to form a porous network, which is indicative of their high surface area and potential for various applications, particularly in sensors and catalysis.

The ZnO nanosheets exhibit an irregular morphology with ultra-thin nanosheets dispersed randomly. This random dispersion contributes to the porous nature of the structure, enhancing the material's surface area and thereby its functional properties. The high porosity is advantageous for applications that require a large surface area, such as gas sensing and photocatalysis, as it allows for more active sites to interact with target molecules or light.

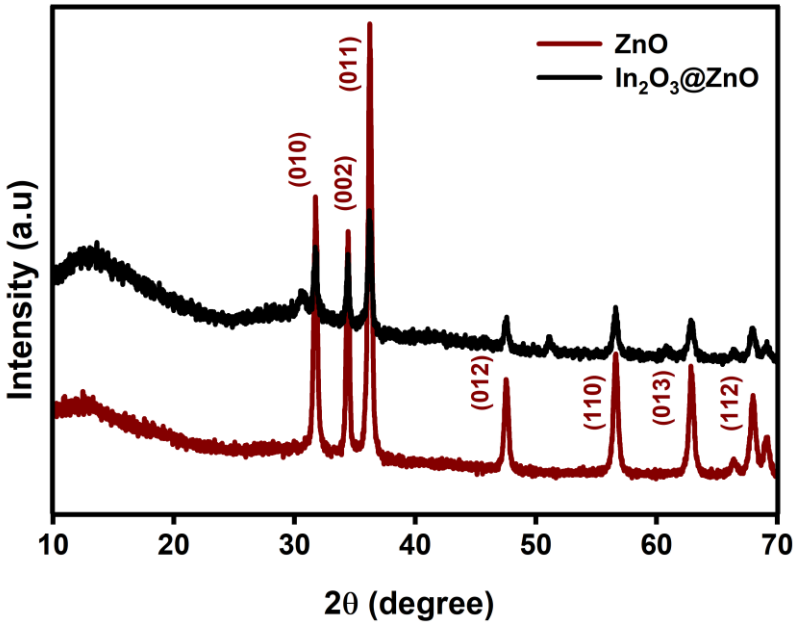

Fig. 2. X r-ray diffraction spectra of ZnO and In_2O_3@ZnO.

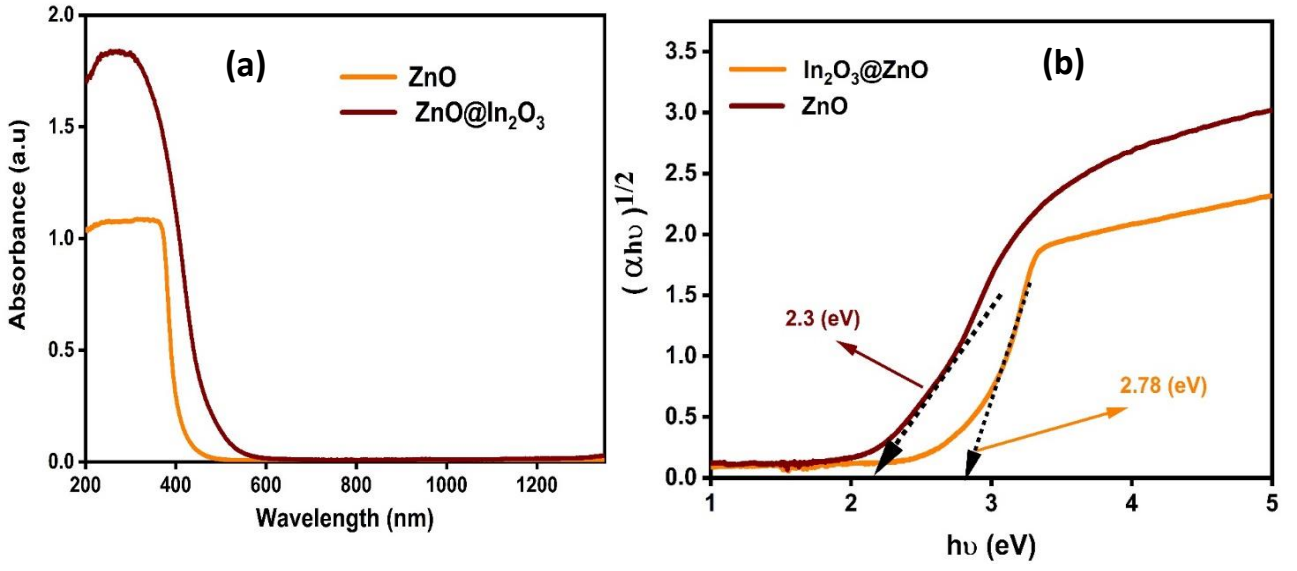

Fig. 3. (a) UV-DRS spectra (b) Tauc's plots and band gap calculation of ZnO and In_2O_3@ZnO.

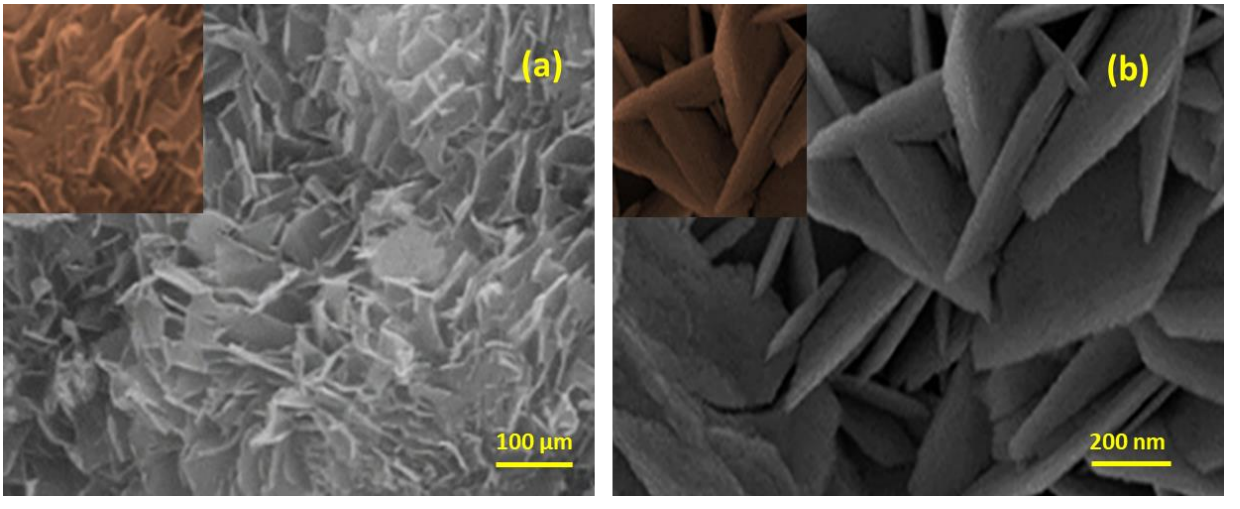

Fig. 4. (a and b) SEM images of In_2O_3@ZnO at different magnifications.

Upon doping with indium, the morphological changes in ZnO are notable. The decoration of In_2O_3 nanoparticles on the sheet-like surface of ZnO is clearly visible in Figure 4a. These In_2O_3 nanoparticles adhere uniformly to the surface of ZnO without altering the overall sheet-like morphology of the ZnO nanosheets. This surface decoration with In_2O_3 not only maintains the original morphology of ZnO but also introduces additional functional sites that can enhance the material's overall performance.

3.4. Gas Sensing Performance

The gas sensing performance of the fabricated sensors was investigated across different operating temperatures, ranging from 100°C to 350°C, as depicted in Figure 5(a). The In_2O_3@ZnO nanosheets (Ns) exhibited a significantly higher response (Rg/Ra = 41.9) compared to pure ZnO Ns (14.04). This indicates that the incorporation of In_2O_3 nanoparticles enhances the detection and response capabilities for NO_2 gas. The response values for both sensors were similar in the temperature range of 100°C to 200°C due to the adsorption of NO_2 nearing saturation. However, as the temperature increased to 300°C, the response of In_2O_3@ZnO Ns reached its maximum value. Beyond 300°C, the response decreased with further temperature increase to 350°C due to thermal energy and diffusion effects. At higher temperatures, gas molecules diffuse more quickly through the sensing material, reducing the interaction time with the surface of In_2O_3@ZnO Ns. This results in a lower gas response as fewer gas molecules effectively interact with the surface of the sensing material. Therefore, 300°C was determined to be the optimal operating temperature, representing the peak efficiency for gas sensors.

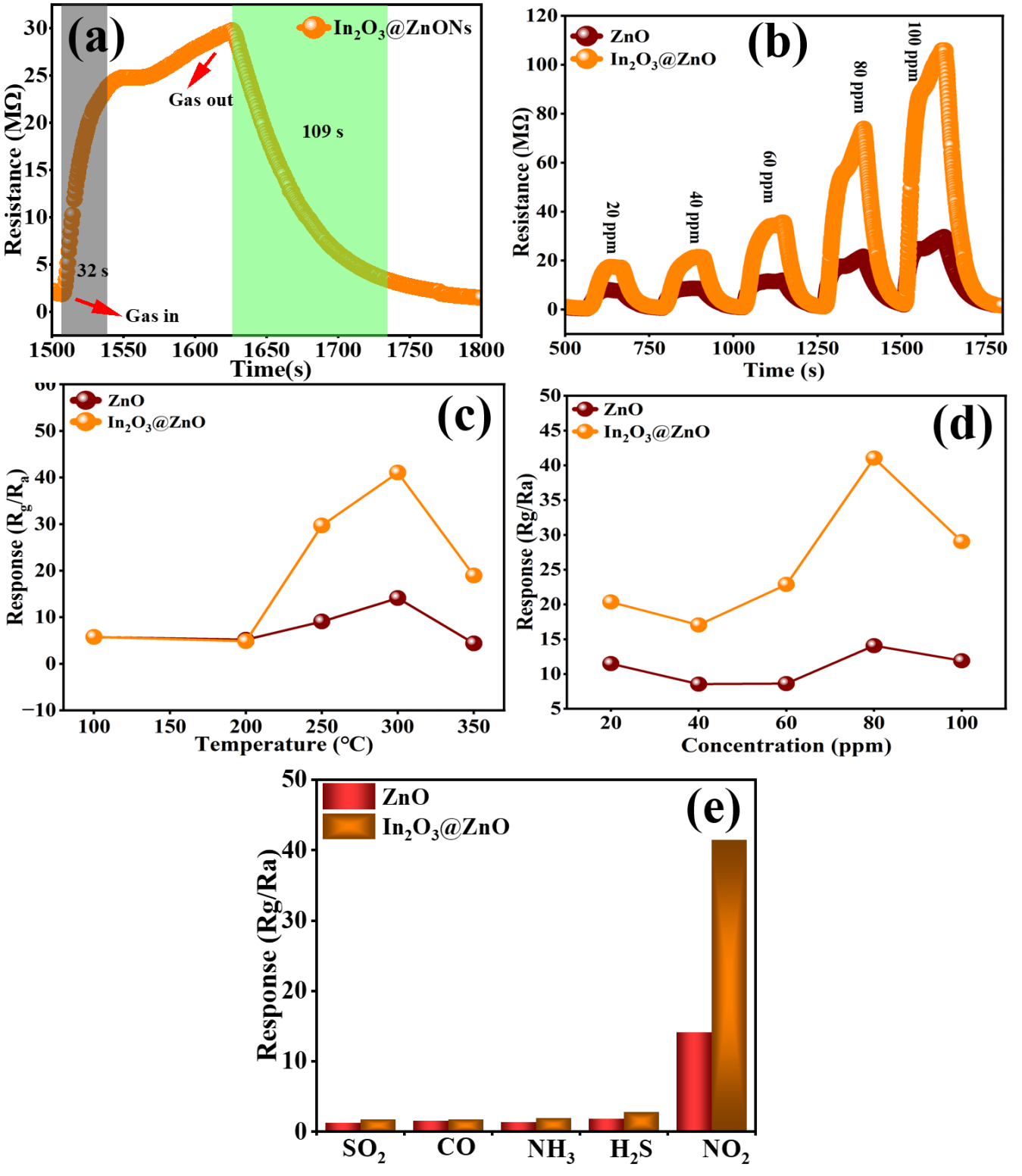

Fig. 5. (a) Responses of sensors to NO_2 at different operating temperatures, (b) Responses of pristine ZnO Ns and In_2O_3@ZnO Ns to various concentration NO_2 at 300 °C, (c) Dynamic resistances of pristine ZnO Ns and In_2O_3@ZnO Ns towards NO_2 at different concentration of ppm; (c) (a) Response and recovery transient curve of In_2O_3@ZnO Ns based sensor at 300 °C to 100 ppm NO_2, (d) Responses of pristine ZnO Ns and In_2O_3@ZnO Ns sensors to different gases at 300 °C temperature.

In_2O_3@ZnO Ns also demonstrated excellent responsiveness to varying NO_2 gas concentrations ranging from 50 ppm to 100 ppm. When exposed to different NO_2 gas concentrations (20, 40, 60, 80, and 100 ppm), the corresponding response values for In_2O_3@ZnO Ns were 22.2, 20.38, 17.04, 22.86, 41.04, and 29.04, respectively, as shown

in Figure 5(b). The responses of pristine ZnO and In_2O_3@ZnO composites were similar, although a slight hysteresis was observed due to the addition of In_2O_3 nanoparticles.

The resistance characteristics of both pristine ZnO and In_2O_3@ZnO sensors in response to various NO_2 concentrations (50 to 100 ppm) are illustrated in Figure 5c. The sensitivity of the gas sensors improved with increasing NO_2 gas concentration. There was a clear increase and decrease in resistance of both sensors with NO_2 gas injection and vice versa. The sensing and response/recovery times were obtained from the alternating change in resistance. The results in Figure 5(c) indicate that the sensitivity value of In_2O_3@ZnO Ns reached 41.9 at 100 ppm NO_2, whereas the response of pristine ZnO Ns was 14.04 at the same concentration.

The effective operation of a gas sensor relies heavily on its response and recovery times, which are crucial for detecting gases. The transient response curve depicting the reaction of In_2O_3@ZnO sensors to 100 ppm NO_2 is shown in Figure 5d. At 300°C and 100 ppm, the response/recovery time for the In_2O_3@ZnO sensor was 32/109 seconds. These gas sensors exhibit considerable promise for monitoring indoor air quality, which is critical in practical scenarios, and are adept at tracing ppm levels of NO_2 gas.

Selectivity is a crucial characteristic for gas sensors as it minimizes sensor failures and enhances application accuracy. An evaluation of the gas sensors was conducted to assess their reactions to five different gases at concentrations of 100 ppm, including sulfur dioxide (SO_2), carbon monoxide (CO), ammonia (NH_3), hydrogen sulfide (H_2S), and nitrogen dioxide (NO_2), as shown in Figure 5e. The results demonstrated that the In_2O_3@ZnO Ns sensor exhibited a more pronounced response to NO2 compared to the other gases. Additionally, the gas sensor constructed with In_2O_3@ZnO Ns showed significantly improved selectivity towards NO_2 gas in contrast to pristine ZnO Ns. At 300°C, the gas sensor response to 100 ppm of NO_2 was recorded at 41.9, which signified a nearly 2.9 times higher response than that of pristine ZnO Ns to NO_2. These findings indicate that In_2O_3@ZnO Ns are highly effective for NO_2 detection, with enhanced sensitivity, selectivity, and optimal operating conditions, making them promising candidates for practical gas sensing applications.

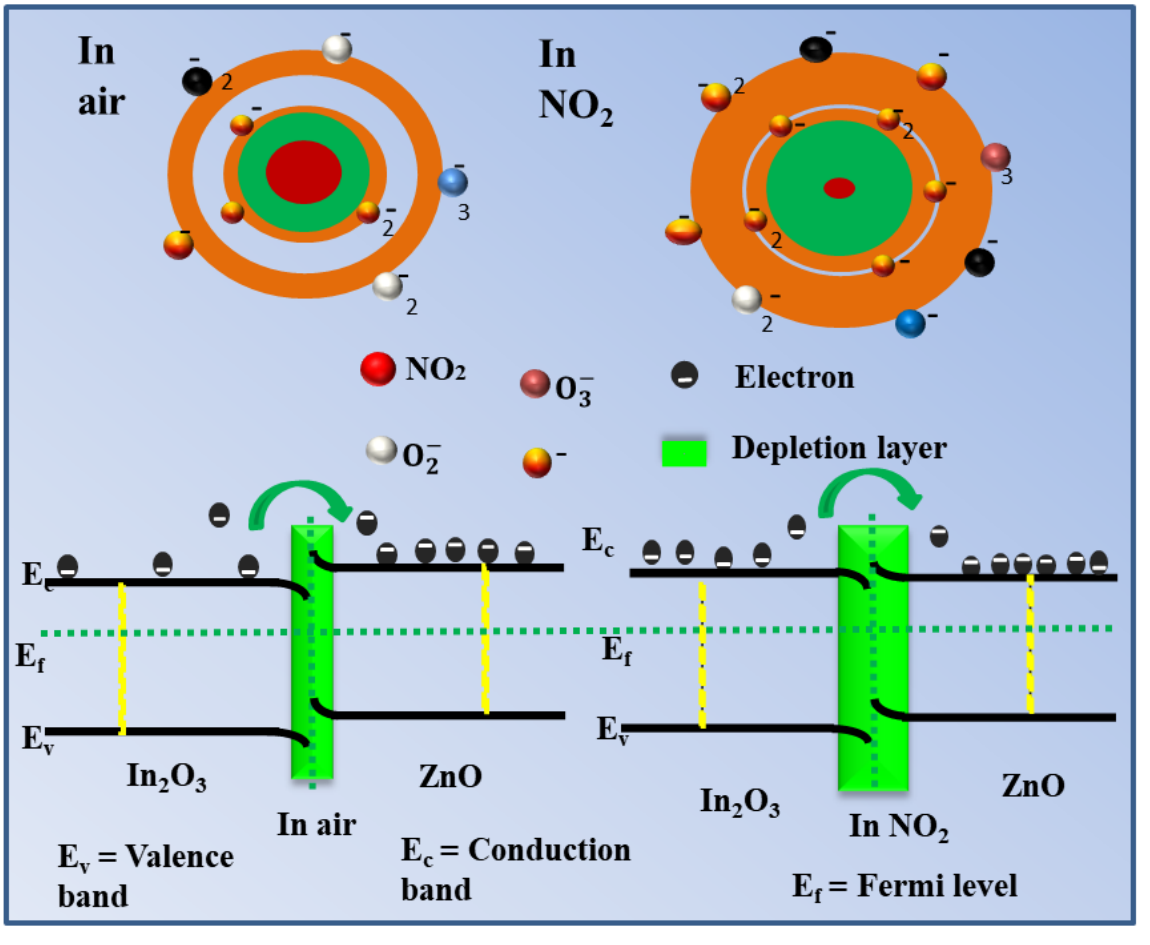

Fig. 6. Schematic diagram of gas sensitivity mechanism of In_2O_3@ZnO in air and NO_2.

3.5. Gas sensing Mechanism

The sensing phenomenon of In_2O_3@ZnO sensor being exposed to atmospheric conditions, resulting in adsorption of O2 gas molecules onto In_2O_3@ZnO Ns surface to generate oxygen species such as (O_2^-, O^{2-}, O^-), serves as conducting channels through capture of unbound electrons from the ZnO conduction band, consequently inducing the creation of an elevated potential barrier on the surface. This process can be expressed by the below equation:

$$O_2 \leftrightarrow \quad O_2^- \leftrightarrow O^- \leftrightarrow O^{2-}$$

When In_2O_3@ZnO nanocomposites gas sensor undergoes testing with NO_2 gas, the gas molecules exhibit a phenomenon where they capture available electrons from oxygen adsorbed on the surface, consequently leading to formation of a substantial charge-depletion layer on In_2O_3@ZnO surface. The presence of active NO_2 molecules in adsorption process initiates a negative charge that activates an elevation in potential barrier on surface. This increased potential barrier subsequently provokes a decline in concentration of charge carriers and electron mobility of sensor, ultimately resulting in a notable increase in electrical resistance [21–23]. Upon exposure of In_2O_3@ZnO nanocomposites to atmosphere, the cavities present on surface interact with NO_2 gas molecules, causing the freedom of electrons into conduction band and release of NO_2 molecules into surrounding air. Consequently, there is a reduction in resistance of In_2O_3@ZnO nanocomposites. The processes of adsorption and desorption taking place on surface of ZnO are explained in following chemical reactions.

$$NO_2(gas)+e^- \rightarrow \quad NO_2^-(ads)$$

$$NO_2^-(ads) + 2e^- + O^-(ads) \rightarrow NO(gas) + 2O^{-2}(ads)$$

During heterojunction of In_2O_3@ZnO nanocomposites, electrons move from conduction band of In_2O_3 to ZnO as a result of high Fermi energy level displayed by In_2O_3, while holes are found to migrate from the valence band of ZnO to In_2O_3 [4, 6]. Consequently, n-n type heterojunctions are formed, leading to creation of interfacial barriers between ZnO and In_2O_3 nanocrystals, thereby enhancing the sensing capabilities of In_2O_3@ZnO nanocomposite sensors [24, 25]. Upon exposure of sensor to oxidized NO_2, a redox reaction is caused between NO_2 molecules and adsorbed oxygen species, following the aforementioned processes. The proposed mechanism of In_2O_3@ZnO nanocomposites for NO_2 gas sensing is illustrated in Figure 6.

4. CONCLUSION

In summary, In_2O_3-doped ZnO nanosheets were successfully prepared using the hydrothermal method and effectively utilized as a gas sensor for the trace detection of NO_2. Various physical characterization techniques confirmed the successful synthesis and the formation of the gas sensor. Morphological studies revealed that the nanosheets exhibited a sheet-like structure with indium nanoparticles adhered to the surface of ZnO, enhancing the sensor's functionality. The gas sensing performance of the In_2O_3@ZnO nanosheets demonstrated excellent sensitivity towards NO_2. The sensor exhibited a rapid response time of 32 seconds, indicating its potential for real-time gas detection applications. Additionally, the sensor showed a good linearity in response to varying concentrations of NO_2, effectively detecting even lower concentrations. This highlights the sensor's ability to provide accurate and reliable measurements across a range of NO_2 levels. Furthermore, the In_2O_3@ZnO nanosheets displayed remarkable stability and repeatability in their gas sensing performance. The sensor maintained consistent responses over multiple cycles, underscoring its reliability for long-term usage. The selectivity of the sensor towards NO_2 was also noteworthy, as it exhibited minimal interference from other gases, making it a robust choice for environmental monitoring. The current study represents a significant step forward in the development of potential gas sensors aimed at monitoring environmental health and ecosystem conditions. The integration of In_2O_3 into ZnO nanosheets has proven to be an effective strategy for enhancing gas sensing properties. Future work may focus on further optimizing the synthesis parameters, exploring additional dopants, and expanding the application scope of these sensors to other hazardous gases. The findings of this study pave the way for the development of advanced, reliable, and efficient gas sensors, contributing to improved environmental monitoring and protection.

CONFLICT OF INTEREST

The authors declare that there is no conflict of interests.

REFERENCES

[1] Ganie, A.S., Bano, S., Khan, N., Sultana, S., Rehman, Z., Rahman, M.M., Sabir, S., Coulon, F. and Khan, M.Z., **2021.** Nanoremediation technologies for sustainable remediation of contaminated environments: Recent advances and challenges. *Chemosphere*, *275*, p.130065.

[2] Zhang, D., Chen, W., Cheng, C., Huang, H., Li, X., Qin, P., Chen, C., Luo, X., Zhang, M., Li, J. and Sun, X., **2023.** Air pollution exposure and heart failure: A systematic review and meta-analysis. *Science of The Total Environment*, *872*, p.162191.

[3] Stieb, D.M., Berjawi, R., Emode, M., Zheng, C., Salama, D., Hocking, R., Lyrette, N., Matz, C., Lavigne, E. and Shin, H.H., **2021.** Systematic review and meta-analysis of cohort studies of long term outdoor nitrogen

dioxide exposure and mortality. *PloS one*, *16*(2), p.e0246451.

[4] Dutta, T., Noushin, T., Tabassum, S. and Mishra, S.K., **2023**. Road Map of Semiconductor Metal-Oxide-Based Sensors: A Review. *Sensors*, *23*(15), p.6849.

[5] Yadav, A.B., Periasamy, C. and Jit, S., **2015.** Study of post annealing effects on structural and optical properties of sol-gel derived ZnO thin films grown on n-Si substrate. In *IOP Conference Series: Materials Science and Engineering* (Vol. 73, No. 1, p. 012060). IOP Publishing.

[6] Raha, S. and Ahmaruzzaman, M., **2022.** ZnO nanostructured materials and their potential applications: progress, challenges and perspectives. *Nanoscale Advances*, *4*(8), pp.1868-1925.

[7] Baruwati, B., Kumar, D.K. and Manorama, S.V., **2006.** Hydrothermal synthesis of highly crystalline ZnO nanoparticles: a competitive sensor for LPG and EtOH. *Sensors and Actuators B: Chemical*, *119*(2), pp.676-682.

[8] Rai, P. and Yu, Y.T., **2012.** Citrate-assisted hydrothermal synthesis of single crystalline ZnO nanoparticles for gas sensor application. *Sensors and Actuators B: Chemical*, *173*, pp.58-65.

[9] Sharmila, B., Singha, M.K. and Dwivedi, P., **2023.** Impact of annealing on structural and optical properties of ZnO thin films. *Microelectronics Journal*, *135*, p.105759.

[10] Cai, Z., Park, J. and Park, S., **2023.** Porous In_2O_3–ZnO nanofiber-based sensor for ultrasensitive room-temperature detection of toluene gas under UV illumination. *Journal of Materials Research and Technology*, *24*, pp.2482-2499.

[11] Wang, S., Wang, X., Qiao, G., Chen, X., Wang, X. and Cui, H., **2021.** Core-double shell ZnO@ In_2O_3@ ZnO hollow microspheres for superior ethanol gas sensing. *Sensors and Actuators B: Chemical*, *341*, p.130002.

[12] Majhi, S.M., Navale, S.T., Mirzaei, A., Kim, H.W. and Kim, S.S., **2023.** Strategies to boost chemiresistive sensing performance of In_2O_3-based gas sensors: an overview. *Inorganic Chemistry Frontiers*, *10*(12), pp.3428-3467.

[13] Cheng, Z., Song, L., Ren, X., Zheng, Q. and Xu, J., **2013.** Novel lotus root slice-like self-assembled In_2O_3 microspheres: synthesis and NO_2-sensing properties. *Sensors and Actuators B: Chemical*, *176*, pp.258-263.

[14] Niu, H., Li, N., Kim, E.S., Shin, Y.K., Kim, N.Y., Shen, G. and Li, Y., **2024.** Advances in advanced solution-synthesis-based structural materials for tactile sensors and their intelligent applications. *InfoMat*, *6*(1), p.e12500.

[15] Kumari, S., Raturi, S., Kulshrestha, S., Chauhan, K., Dhingra, S., András, K., Thu, K., Khargotra, R. and Singh, T., **2023.** A comprehensive review on various techniques used for synthesizing nanoparticles. *Journal of Materials Research and Technology*. 27, pp. 1739-1763.

[16] Huang, C., Chen, X., Xue, Z. and Wang, T., **2020.** Effect of structure: A new insight into nanoparticle assemblies from inanimate to animate. *Science Advances*, *6*(20), p.eaba1321.

[17] Gómez-Gómez, A.L., Martínez-Ayala, A.L., Moguel-Concha, D.D.R., Borges-Martínez, J.E., Perea-Flores, M.D.J. and Dávila-Ortiz, G., **2023.** Relationship of nanomaterials' structure based on their application in the food industry: physicochemical and techno-functional characteristics. *Applied Sciences*, *13*(12), p.7167.

[18] Masoumi, S., Shokrani, M., Aghili, S. and Hossein-Babaei, F., **2019.** Zinc oxide-based direct thermoelectric gas sensor for the detection of volatile organic compounds in air. *Sensors and Actuators B: Chemical*, *294*, pp.245-252.

[19] Shah, S., Hussain, S., Qiao, G., Tan, J., Javed, M.S., Zulfiqar, Ge, C., Wang, M. and Liu, G., **2020.** Decorating spherical In_2O_3 nanoparticles onto ZnO nanosheets for outstanding gas-sensing performances. *Journal of Materials Science: Materials in Electronics*, *31*, pp.3924-3933.

[20] Li, T.T., Bao, N., Geng, A.F., Yu, H., Yang, Y. and Dong, X.T., **2018.** Study on room temperature gas-sensing performance of CuO film-decorated ordered porous ZnO composite by In_2O_3 sensitization. *Royal Society open science*, *5*(2), p.171788.

[21] Shah, S., Hussain, S., Din, S.T.U., Shahid, A., Amu-Darko, J.N.O., Wang, M., Tianyan, Y., Liu, G. and Qiao, G., **2024.** A Review on In_2O_3 Nanostructures for Gas Sensing Applications. *Journal of Environmental Chemical Engineering*, p.112538.

[22] Goel, S., Sinha, N., Yadav, H., Joseph, A.J. and Kumar, B., **2017.** Experimental investigation on the structural, dielectric, ferroelectric and piezoelectric properties of La doped ZnO nanoparticles and their application in dye-sensitized solar cells. *Physica E: Low-dimensional Systems and Nanostructures*, *91*, pp.72-81.

[23] Shah, S., Han, S., Hussain, S., Liu, G., Shi, T., Shaheen,

A., Xu, Z., Wang, M. and Qiao, G., **2022.** NO_2 gas sensing responses of In_2O_3 nanoparticles decorated on GO nanosheets. *Ceramics International*, *48*(9), pp.12291-12298.

[24] Park, S., Jung, Y.W., Ko, G.M., Jeong, D.Y. and Lee, C., **2021.** Enhanced NO_2 gas sensing performance of the In_2O_3-decorated SnO_2 nanowire sensor. *Applied Physics A*, *127*, pp.1-12.

[25] Goel, S., Sinha, N., Yadav, H., Godara, S., Joseph, A.J. and Kumar, B., **2017.** Ferroelectric Gd-doped ZnO nanostructures: enhanced dielectric, ferroelectric and piezoelectric properties. *Materials Chemistry and Physics*, *202*, pp.56-64.